Ayoub, A. & Filippou, F. C. (2010). Finite-Element Model for Pretensioned Prestressed Concrete Girders. Journal of Structural Engineering, 136(4), pp. 401-409. doi: 10.1061/(ASCE)ST.1943-541X.0000132, 401-409

A FINITE ELEMENT MODEL FOR PRETENSIONED PRESTRESSED CONCRETE GIRDERS

By Ashraf Ayoub, A.M. ASCE[1], and Filip C. Filippou, M. ASCE[2]

Abstract

This paper presents a nonlinear model for pretensioned prestressed concrete girders. The model consists of three main components: a beam-column element that describes the behavior of concrete, a truss element that describes the behavior of prestressing tendons, and a bond element that describes the transfer of stresses between the prestressing tendons and the concrete. The model is based on a two-field mixed formulation, where forces and deformations are both approximated within the element. The nonlinear response of the concrete and tendon components is based on the section discretization into fibers with uniaxial hysteretic material models. The stress transfer mechanism is modeled with a distributed interface element with special bond stress-slip relation. A method for accurately simulating the prestressing operation is presented. Accordingly, a complete nonlinear analysis is performed at the different stages of prestressing. Correlation studies of the proposed model with experimental results of pretensioned specimens are conducted. These studies confirmed the accuracy and efficiency of the model.

CE Database subject headings: Prestressed concrete; Pretensioning; Finite element method; Nonlinear analysis; Bond stress; Slip.

---

[1] Associate Professor, University of Houston, Houston, TX 77204

[2] Professor, University of California at Berkeley, Berkeley, CA 94720

Introduction

The use of prestressed concrete in the design of buildings, bridges, tanks, offshore platforms and many other structures has increased dramatically since the second world war. The active combination of high strength concrete and high strength steel leads to the achievement of desirable structural properties such as high strength to weight ratio, increased flexural ductility, improved shear strength, better deformation control and deformation recovery with crack closure upon unloading. These properties have made prestressed concrete the ideal choice for many structural applications.

Two different procedures for prestressing exist: pretensioning procedures, and post-tensioning procedures. The main difference between pretensioned and post-tensioned structures is the type of prestressing. The term pretensioning is used to describe any method of prestressing in which the tendons are tensioned before the concrete is placed. The tendons must be temporarily anchored against an abutment or stressing bed when tensioned, and the prestress is transferred to the concrete after the concrete has set. The tendons generally have their prestress transmitted to the concrete by their bond action near the beam ends. The effectiveness of such stress transmission is limited to large diameter strands which possess better bond properties than smooth wires. Pretensioning was developed by the German engineer E. Hoyer as a practical technique in 1938, and is employed in precasting plants or laboratories where permanent beds are provided for such tensioning, and in fields where abutments can be economically constructed. The term post-tensioning, on the other hand, is used when the tendons are stressed against the concrete after it has hardened.

Modeling of prestressing tendons in finite element analysis can be performed in two ways, as discussed by Aalami (2000), either as a loading applied to the member, or as an additional structural element that contributes to the resistance to the applied loads. The first considers the prestressing effects just as loads acting on the concrete member. The load is applied either using load balancing techniques (e.g. Aalami 1990), through applied primary and secondary moments (e.g. Picard et. al. 1995), or by discretization of the tendon force (e.g. ADAPT-PT 1999). The main drawback of this method is that it neglects the effect of the concrete deformation on the prestressing force, and thus doesn't predict the prestressed losses accurately. In the second method, the tendon is modeled as an additional load resisting element, and contributes to the overall stiffness of the structure. Such technique directly takes into account the interaction between the tendon and its surrounding concrete. Furthermore, long term effects could be directly accounted for in this type of modeling without separate stress loss calculations.

In the second method of analysis, most previously developed formulations are based on the displacement method of analysis (e.g. Kang 1977; Mari 1984; Roca and Mari 1993, and Cruz et al. 1998). In this method, typically a linear variation of axial deformation and a cubic variation of transverse deformation are assumed along the element length. For pre-tensioned constructions, prestressing tendons are modeled as steel segments perfectly bonded to the concrete beam. The prestressing operation is simulated simply by transferring the prestressing force in the tendon to the concrete reference axis.

The main shortcoming of displacement formulations lies in their inability to accurately trace localized curvature distributions in the plastic zone, since they typically assume linear interpolation functions for curvatures. A fine mesh is thus needed in the

plastic area, which renders the problem computationally expensive. Furthermore, all previously developed models assumed perfect bond between prestressing tendons and concrete and neglected slip effects. It is known that for pre-tensioned structures, tendons are anchored to the concrete by direct bond, which depends on several factors including among other concrete quality, surface roughness of the prestressing steel and size of strands. The prestressing force is transferred from the steel tendon to the concrete over a specified transfer length that depends on the bond properties between tendon and concrete. Estimation of the value of the transfer length is essential for design purposes, and failure to evaluate it properly can lead to unsafe designs. It is therefore necessary to include bond-slip effects in finite element models to account for such an important phenomenon.

Another method of modeling pre-tensioned beams is based on the force method of analysis (e.g. Kodur 1988, Yassin 1994). In this method, equilibrium is satisfied within the element in a strong sense. Kodur used a curvature incrementing technique using pre-generated moment-curvature relations to trace the behavior of bonded prestressed beams. For each increment of curvature, a secant stiffness is used to determine the moment and curvature in each segment. The moment is checked against the one determined from the pre-generated moment-curvature relation, and the cycle is repeated until convergence is satisfied. One limitation of the model is that moment equilibrium is checked only at the central section of a segment. The use of a single control point per segment does not allow for accurately estimating the plastic hinge length of the beam, and hence the failure load. Another shortcoming of the model by Kodur is that it also neglected bond-slip and transfer length effects.

The model by Yassin (1994) is also based on the force method of analysis. The model considers bond-slip effects, and uses force-based beam elements (Spacone et. al. 1996) to describe concrete behavior, and truss elements to describe tendon behavior. Bond stresses are assumed to follow a linearly varying distribution, which results in a set of distributed loads acting on both the concrete beam and the tendon. The transfer of prestress is simulated by performing a complete nonlinear analysis for each stage of the prestressing operation. While the model by Yassin is the first to consider bond effects and transfer length in modeling pre-tensioned beams, its main shortcoming lies in the fact that it evaluates the bond stiffness and resisting loads at element ends only. This lumping procedure requires a fine mesh in regions of high bond stresses, which increases the computational cost of the solution.

This paper presents a new model for pretensioned prestressed concrete beams. The model uses the same approach of Yassin (1994) for simulating the prestressing operation, but overcomes most of its numerical limitations by adopting a two-field mixed formulation for the finite element solution of the problem. The new model is described next.

Prestressed Concrete Beam Model

The model for the prestressed concrete element is made up of three components: (a) a fiber beam-column element, (b) a tendon element, and (c) a bond element. The fiber beam-column element describes the behavior of concrete and bonded mild reinforcement. The tendon element describes the behavior of the prestressing steel tendon. The bond element describes the transfer of forces between the prestressing tendon and the fiber

beam-column element. The interaction between the beam-column and the tendon elements, which together form a parallel system, is such that the transfer of forces between them occurs continuously along their lengths through the bond element. The bond element describes the interaction between the beam-column and tendon elements with special bond stress-slip relations. The total number of degrees of freedom for each prestressing element node equals the number of degrees of freedom for the concrete beam node, in addition to the number of prestressing tendons.

In the nonlinear analysis of pretensioned beams, it is important that the prestressing operation be simulated as accurately as possible. This is because the different stages of the operation will result in different initial stress distributions, thus affecting the overall behavior. Aspects of structural behavior such as the occurrence of secondary moments, initial deformations due to prestress, and prestress losses are very much influenced by the method of prestressing. Therefore, the simulation of the different stages of prestressing is essential in capturing the most relevant aspects of the structural behavior.

The finite element model for the pretensioned prestressed concrete beam used in this study is based on a newly developed mixed formulation, where both, forces and deformations, are approximated within the element. The formulation is modified to account for the simulation of the prestressing operation at the initial stages. In the next section, the finite element model for pretensioned prestressed concrete beams is briefly presented followed by a discussion of the prestressing operation. The model for the pretensioned prestressed concrete beam is implemented in the general purpose finite element program FEAP developed by R.L. Taylor and described in Zienkiewicz and Taylor (1989).

Finite Element Model for Pretensioned Prestressed Concrete Beams

In the mixed formulation, the differential equations are solved with the interpolation of both the displacement and the force field. A detailed derivation of the formulation is presented in earlier studies by Ayoub and Filippou (1999) for anchored reinforcing bar problems, Ayoub and Filippou (2000) for composite steel-concrete beam elements, and Ayoub (2006) for reinforced concrete beam-columns with bond-slip. The present mixed model for prestressed beams is similar in concept. Accordingly, the equilibrium equation of a prestressed beam with J tendons can be written, similar to the latter study, as:

$$\mathbf{L}^T \boldsymbol{D}(x) - \mathbf{L}_b^T \boldsymbol{\rho} \mathbf{q}_b(x) = \mathbf{w} \tag{1}$$

where $\boldsymbol{D}(x) = \left[N_c(x) \quad \ldots \quad N_{sj}(x) \quad \ldots \quad M(x) \right]^T$ j=1,J,

N_c and N_{sj} are the axial forces in the concrete and jth tendon respectively, M is the bending moment, $\mathbf{L}$ is a differential operator that includes first derivative of the axial parameters and second derivative of the flexural parameters,

$\mathbf{L}_b = \begin{bmatrix} \ldots & \ldots & & \ldots \\ -1 & & 1 & h_j d/dx \\ \ldots & & \ldots & \ldots \end{bmatrix}$ is a $J \times J+2$ differential operator, h_j is the distance between the centroid of the concrete beam and the jth tendon, $\boldsymbol{\rho}$ is a diagonal matrix that includes the tendons perimeter,

$\mathbf{q}_b(x) = \left[\ldots \quad q_{bj}(x) \quad \ldots \right]^T$, q_{bj} is the bond stress for the jth tendon, and $\mathbf{w}$ is the vector of externally applied distributed loads. Similarly, the compatibility equation is:

$$\mathbf{L}\boldsymbol{u}(x) - \boldsymbol{d}(x) = 0 \tag{2}$$

where $\boldsymbol{u}(x) = \left[u_c(x) \quad ... \quad u_{sj}(x) \quad ... \quad v(x)\right]^T$, u_c and u_{sj} are the concrete and *j*th tendon axial displacement respectively, v is the vertical displacement of the beam,

$\boldsymbol{d}(x) = \left[\varepsilon_c(x) \quad ... \quad \varepsilon_{sj}(x) \quad ... \quad \chi(x)\right]^T$, ε_c and ε_{sj} are the concrete and *j*th tendon axial strains respectively, and χ is the beam curvature.

The present model uses fiber discretization to describe section behavior, and a distributed interface element to model bond behavior. The section and bond constitutive laws are:

$$\boldsymbol{D}(x) = f_{\text{sec}}\left[\boldsymbol{d}(x)\right], \qquad q_b(x) = f_{bond}\left[S_b(x)\right] \tag{3}$$

where f_{sec} is a nonlinear function that describes the section force deformation response through fiber integration, where the fibers are either steel or concrete; and f_{bond} is a nonlinear function that describes the relationship between the bond stress $q_b(x)$ and bond slip $S_b\ (x)$.

Material constitutive laws for the three main components of the pretensioned prestressed element, namely steel, concrete and bond have to be accurately determined. The concrete uniaxial constitutive law used is based on the model by Kent and Park (1971). The steel uniaxial stress-strain law used is based on the model by Menegotto and Pinto (1973) as modified by Filippou et al. (1983). The bond model used in this study is based on the bond stress-slip relation by Eligehausen et al. (1983) for anchored reinforcing bars.

The mixed finite element formulation for a single Newton-Raphson iteration denoted by *i* starts by considering the inverse of the section force-deformation relation:

$$\boldsymbol{d}^i = \mathbf{f}_\mathbf{s}^{i-1}\Delta\boldsymbol{D}^i + \boldsymbol{d}^{i-1} \tag{4}$$

Where $\boldsymbol{d}^{i-1}$ is the section deformation at the end of the last iteration, $\mathbf{f_s}^{i-1}$ the corresponding section flexibility, and Δ represents increments. Substituting (4) in the weighted form of the compatibility equation (2) yields:

$$\int_0^L \delta \boldsymbol{D}^T(x) \left[\mathbf{L}\boldsymbol{u}^i(x) - \mathbf{f_s}^{i-1} \Delta \boldsymbol{D}^i - \boldsymbol{d}^{i-1} \right] dx = 0 \tag{5}$$

where $\delta \boldsymbol{D}(x)$ is the virtual force field in the role of a weight function and the integration extends over the element length L.

The displacement field $\boldsymbol{u}(x)$ and internal force vector $\boldsymbol{D}(x)$ are respectively approximated along the beam length through the displacement shape functions $\mathbf{a}(x)$ and force interpolation functions $\mathbf{b}(x)$:

$$\boldsymbol{u}(x) = \mathbf{a}(x)\,\mathbf{v}, \qquad \boldsymbol{D}(x) = \mathbf{b}(x)\,\mathbf{q} \tag{6}$$

where $\mathbf{v}$ and $\mathbf{q}$ are the vector of element end displacements and forces respectively. In this work, cubic hermitian polynomials and quadratic functions are used to approximate the transverse and axial displacements respectively, while linear functions are used to approximate the axial forces and external bending moments.

Substituting $\mathbf{a}(x)$ and $\mathbf{b}(x)$ into (5), results in

$$\mathbf{T}\,\Delta\mathbf{v}^i - \mathbf{F}^{i-1}\Delta\mathbf{q}^i - \mathbf{v_r}^{i-1} = 0 \tag{7}$$

$$\mathbf{T} = \int_0^L \mathbf{b}^T(x)\mathbf{B}(x)dx, \quad \mathbf{F}^{i-1} = \int_0^L \mathbf{b}^T(x)\mathbf{f_s}^{i-1}(x)\,\mathbf{b}(x)dx, \quad \mathbf{v_r}^{i-1} = \int_0^L \mathbf{b}^T(x)\,\boldsymbol{d}^{i-1}(x)\,dx - \mathbf{T}\,\mathbf{v}^{i-1} \tag{8}$$

$\mathbf{B}(x) = \mathbf{L}\mathbf{a}(x)$, $\mathbf{L}$ is defined in (1), $\mathbf{F}$ is the beam flexibility matrix and $\mathbf{v}_r^{i-1}$ is the vector of nodal displacement residuals at the end of the previous iteration.

The weighted integral form of the equilibrium equation is:

$$\int_0^L \delta \boldsymbol{u}^T(x)\left[\mathbf{L}^T \boldsymbol{D}^i(x) - \mathbf{L}_\mathbf{b}^T \boldsymbol{\rho} \mathbf{q}_b^i(x) - \mathbf{w}\right] dx = 0 \tag{9}$$

where $\delta \boldsymbol{u}(x)$ is a weighting function. For the sake of simplicity the effect of element loads **w** is neglected in this study. Integrating by parts twice the first term in (9), and substituting the incremental force-deformation relation of the bond $\mathbf{q}_b^i = \boldsymbol{k}_b^{i-1} \Delta \boldsymbol{S}_b^i + \mathbf{q}_b^{i-1}$, where $\boldsymbol{k}_b$ is the tangent to the bond stress-slip nonlinear function, we get:

$$\int_0^L \mathbf{L}^T \delta \boldsymbol{u}^T(x)\, \boldsymbol{D}^i(x)\, dx + \int_0^L \mathbf{L}_\mathbf{b}^T \delta \boldsymbol{u}^T(x)\left[\boldsymbol{\rho} \boldsymbol{k}_b^{i-1} \Delta \boldsymbol{S}_b^i + \boldsymbol{\rho} \mathbf{q}_b^{i-1}\right] dx = \mathrm{BT} \tag{10}$$

where BT is the boundary term. Substituting the predefined displacement shape functions and force interpolation functions into (10) yields

$$\mathbf{T}^T \Delta \mathbf{q}^i + \mathbf{K}_\mathbf{b}^{i-1} \Delta \mathbf{v}^i = \mathbf{P} - \mathbf{T}^T \mathbf{q}^{i-1} - \mathbf{q}_\mathbf{b}^{i-1} \tag{11}$$

where **T** is as defined in (8), $\mathbf{K}_\mathbf{b}^{i-1} = \int_0^L \mathbf{B}_\mathbf{b}{}^T(x)\, \boldsymbol{\rho} \boldsymbol{k}_b^{i-1}\, \mathbf{B}_\mathbf{b}\, dx$ is the contribution of the bond to the element stiffness, $\mathbf{B}_b(x) = \mathbf{L}_b \mathbf{a}(x)$, $\mathbf{q}_\mathbf{b}^{i-1} = \int_0^L \mathbf{B}_\mathbf{b}{}^T(x)\, \boldsymbol{\rho} \mathbf{q}_b^{i-1}(x)\, dx$ is the contribution of the bond to the element resisting forces, and **P** is the vector of applied nodal forces.

Writing equations (7) and (11) in matrix form:

$$\begin{bmatrix} -\mathbf{F}^{i\text{-}1} & \mathbf{T} \\ \mathbf{T}^T & \mathbf{K}_\mathbf{b}^{i\text{-}1} \end{bmatrix} \begin{bmatrix} \Delta \mathbf{q}^i \\ \Delta \mathbf{v}^i \end{bmatrix} = \begin{bmatrix} \mathbf{v}_\mathrm{r}^{i\text{-}1} \\ \mathbf{P} - \mathbf{T}^T \mathbf{q}^{i\text{-}1} - \mathbf{q}_\mathbf{b}^{i\text{-}1} \end{bmatrix} \tag{12}$$

In the mixed model, the element nodal forces $\Delta \mathbf{q}$ in (12) are condensed out at the element level resulting in a generalized stiffness matrix as follow:

$$\mathbf{T}^T \left[\mathbf{F}^{i-1}\right]^{-1} \left[\mathbf{T} \Delta \mathbf{v}^i - \mathbf{v}_\mathbf{r}^{i-1}\right] + \mathbf{K}_\mathbf{b}^{i-1} \Delta \mathbf{v}^i = \mathbf{P} - \mathbf{T}^T \mathbf{q}^{i-1} - \mathbf{q}_\mathbf{b}^{i-1} \tag{13}$$

The process for evaluating the generalized stiffness matrix requires an internal element iteration in addition to the Newton-Raphson iteration, in order to zero the residual deformation vector $\mathbf{v}_r$ as described in Ayoub and Filippou (1999).

The simulation of the prestressing operation mainly involves modifying the vector of externally applied load **P** defined previously, to account for the different stages of prestressing. The prestressing operation is carried out in different stages. In every stage, each component of the prestressed concrete element, namely the fiber beam-column element, the tendon elements and the bond elements, is assumed to be either active or inactive. The term active means that the specific component contributes to the overall element stiffness, and thus has stiffness and resisting load terms in the corresponding structural quantities. The term inactive means that the specific component does not contribute to the overall element stiffness, and thus its stiffness and resisting load terms equal zero. In the next section, modeling of the pretensioning operation will be presented.

Pretensioning Operation

The analysis of a prestressed concrete structure is carried out at discrete times. Each time step represents a specific stage of the prestressing operation. The pretensioning operation is performed in two stages: (a) the tendon tensioning at time t_0, and (b) the transfer of prestress to concrete at time t_1. As shown in Table (1) and Figure (1), in the first stage of pretensioning operation, only the tendon elements are activated. In addition to the prestressed concrete elements there is also a bedding element that is represented by a linear stiff spring with one end fixed and the other end connected to a node. While linking the bedding element node to end node 1 of the tendon, a tensioning force is

applied to end node 2 of the tendon. Accordingly, the tensioning force is added to the load vector **P**. After the completion of the analysis at this stage, the tendon elements will have constant tensile force equal to the tensioning force. The situation models exactly the actual tendon tensioning in a stressing bed.

During the second stage of the pretensioning operation, the beam-column and bond elements are activated. The tensioning force at end node 2 of the tendon is then reduced to zero to simulate the cutting of the strands, and the bedding element at end node 1 of the tendon is removed. The tendon force in the load vector **P** is modified accordingly. In addition, the prestress in the tendon elements is transferred to the beam-column elements via the bond elements. Depending on the resulting bond slip and beam-column deformation, the amount of prestress loss in the tendon varies along the length of the beam. Figure (2) shows the typical analytical tendon force distribution during the two stages of pretensioning, while Figure (3) shows the corresponding analytical bond stress distribution after transfer of prestress. The maximum prestress loss occurs at the ends of the tendon where the tendon force is reduced to zero. The maximum bond slip and bond stress also occurs at the ends of the tendon.

The bond stress-slip relation used for both the prestress transfer bond and the flexural bond follows the same trend, and is based on approximate values given by Tabatabai and Dickson (1993). Such assumption is considered correct because both types of bond are derived from the same physical source, that is the interaction between the tendon and the surrounding concrete. Any load application after the completion of the pretensioning operation will result in bond stress increments additional to the prestress

transfer bond stress. The distributions of tendon force and bond stress obtained thus far have proven to be realistic when compared to experimental results as described next.

Numerical Example: Pre-tensioned Concrete Beams by Mitchell et al. (1993)

Mitchell et al. (1993) tested a series of pretensioned concrete beams to investigate the influence of concrete strength on the transfer length and development length of pretensioning strands. Two of the beams are selected for this study. The dimensions and loading arrangements of the test beams are shown in Figure (4).

Each beam contained a single 15.7 mm diameter low relaxation strand having an ultimate strength of 1793 MPa and a yield strength of 1639.3 MPa. The elastic modulus was 204.9 GPa with a strain hardening ratio of 0.028. Each beam had identical cross section dimensions, with the center of the strand located 50 mm above the bottom face. The material properties and reinforcement details of the test beams are listed in Table (2). f_c' is the compressive strength of concrete, f_t' is its tensile strength, A_p and P_p are the area and perimeter of the strand respectively, and f_{pi} is the initial prestress in the strand prior to transfer. No tension stiffening effect was considered in the analysis.

The strand was instrumented with electrical resistance strain gauges to monitor its strains. The strand was released in a gradual manner by slowly reducing the pressure in the hydraulic stressing rams. The testing of each beam was carried out with either a single-point load or with two-point loads, as shown in Figure (4). Each beam was supported on 100 mm long, 13 mm thick neoprene bearing pads at each end.

The finite element models used for the analysis consist of 6 prestressed concrete finite elements per half span for the first beam and 7 elements per half span for the second

beam. The cross section of the beam-column element is made up of 10 concrete layers at 5 control sections. Model analysis is carried out under displacement control.

The bond parameters used for the analysis are shown in Figure (5), and are based on approximate data given by Tabatabai and Dickson (1993).

The transfer length of the strand is the distance from the end of the member over which the stress in the strand builds up to the effective stress. The flexural bond length is the distance over which the stress in the strand builds up from the effective stress to the maximum stress at ultimate strength of the member. The development length is the sum of the transfer and flexural bond length.

Figure (6) shows the analytical global load-displacement response for beam 16/31-1865. No similar experimental plot is given in the reference. Before the application of the load, the displacement shows a negative value, referred to as camber, which is due to the prestressing force. Yielding of the tendon starts at a load value that equals 32 kN. The specimen then shows a ductile behavior. Figure (6) also shows the response of the beam if perfect bond is assumed between the tendon and concrete. This was obtained using a regular fiber-based beam element in which the prestressing was simulated with an initial strain applied to the tendon. In this case, the camber at transfer is much larger due to the higher prestressing activities taking place near the supports. However, the stiffness and strength are also larger than in the case of bond-slip. Figure (7) shows the strains measured by the strain gauges glued to the prestressing strand in beam 16/31-1865 at different load levels. The maximum measured strand strain was 0.0187, which corresponds to a stress in the strand of 1716 MPa. This beam failed by flexural crushing at a maximum moment of 46.6 kNm (P=51.35 kN). The distribution of the main

parameters of the problem, namely the strand strain, the strand stress, the slip, the bond stress and the curvature, using the proposed model are shown in Figures (8) to Figure (14) at different load stages. In order to allow for proper comparison with the experimental data, these load stages correspond to the load values of Figure (7), and are identified in the above mentioned global response of Figure (6).

The distribution of the strand strain shown in Figure (8) shows that the transfer and development lengths of the strand are very well estimated by the model. However the effective strand strain after transfer is slightly overestimated. This is mainly due to the fact that the model does not take into account long term prestress losses due to concrete creep and shrinkage. Such losses are significant in this case as a result of the relatively low concrete strength, and the fact that testing was performed at age of 65 days. In addition, the dead weight of the beam was ignored in the analysis, which would have further contributed to that discrepancy. The strain at ultimate loads is localized in the region near the midspan, where the maximum bending moment occurs. The analytical strand force distribution after transfer shown in Figure (9) follows the same trend as the corresponding analytical strand strain distribution, and the maximum value is slightly less than the initial prestressing force due to elastic shortening. The analytical strand force distribution shows the build up of strand force due to flexure up to the ultimate load. After the onset of yielding, there is minimal change in strand force distribution up to the ultimate load. Figure (10) shows the strand force distribution if perfect bond was assumed between the concrete and tendon. At transfer, the strand force is constant along the entire beam length, and is also slightly less than the initial prestressing force due to elastic shortening. The strand force distribution at higher load levels is quite different than in the

case of bond-slip, since the build up of force due to flexure starts from the initial transfer force. Figure (11) shows the curvature distribution. The curvature localization in the region near midspan is successfully described by the model. The slip and bond stress distributions are shown in Figures (12) and (13) respectively for all load stages of Figure (6). The slip is maximum at the beam ends, and zero at the midspan. The bond stress distribution after transfer shows almost constant maximum bond stress occurring within the transfer lengths, and low values for the remaining part of the strand. Therefore, bond slip during transfer is confined to the portion of the strand within the transfer length. The bond stress at ultimate loads shows a considerable increase due to the increase in tendon strain in the region near the midspan. Figure (14) shows the concrete strain distribution at the very bottom fiber of the section, along with the assumed cracking strain. The figure could be used to identify the cracked region along the beam length at different load levels.

Figure (15) shows the global load-displacement response for beam 16/65-1150. As in the case of the first test beam, a camber is observed due to prestressing. Yielding of the steel starts at a load level that equals 40 kN, and the behavior afterward becomes ductile. Figure (16) shows the strand force distributions. The build up of the strand force due to flexure is consistent with the bending moment distribution. Figure (17) shows the experimental steel strain distributions. The maximum measured strand strain is 0.022, which corresponds to a stress in the strand of 1732 MPa. This beam failed by flexural crushing at a maximum moment of 49.2 kNm (P=44.73 kN). The analytical strain distribution is shown in Figure (18). The comparison between the analytical and experimental distributions shows that the transfer and development lengths are estimated well by the model. The strains at ultimate loads are localized and have a constant value in

the constant moment region in between the loads. The slip and bond stress distributions are shown in Figures (19) and (20) respectively for all load stages. As for the previous test beam, the slip is maximum at the end beam, and zero at the midspan, and the bond stress distribution after transfer shows almost constant maximum bond stress occurring within the transfer lengths, and low values for the remaining part of the strand. The bond stress at the ultimate load shows a considerable increase due to the increase in tendon strain in the constant moment region near the midspan. Figure (21) shows the curvature distribution. The curvature is localized and has a constant value in the constant moment region in between the loads.

Conclusion

A model for inelastic analysis of pretensioned prestressed concrete beams is presented. The model is derived from a two-field mixed formulation with independent approximation of forces and displacements. The nonlinear response of the concrete and tendons is based on discretization of the section into fibers with uniaxial hysteretic material models. Bond between the concrete and tendons is modeled with a distributed interface element that uses specific bond stress-slip relations. The model ignores though the effect of dead weight, prestress losses, and concrete tension stiffening. Simulation of the prestressing operation is accounted for by carrying out the analysis at several time steps, each representing a specific stage of the operation. Correlation studies with experimentally tested pretensioned beams are performed. The studies confirmed the accuracy and efficiency of the proposed model.

References

ADAPT-ABI software manual (1999). ADAPT Corp., Redwood City, Calif.

Aalami, B, O. (1990). "Load balancing-A comprehensive solution to post-tensioning", ACI Structural Journal, 87(6), 662-670.

Aalami, B, O. (2000). "Structural modeling of post-tensioned members", Journal of Structural Eng., ASCE, 126(2), 157-162.

Ayoub, A.S., and Filippou, F.C. (1999). "Mixed formulation of bond slip problems under cyclic loads", Journal of Structural Eng., ASCE, 125(6), 661-671.

Ayoub, A.S., and Filippou, F.C. (2000). "Mixed formulation of nonlinear steel-concrete composite beam element", Journal of Structural Eng., ASCE, 126(3), 371-381.

Ayoub, A.S. (2006). "Nonlinear analysis of reinforced concrete beam-columns with bond-slip", Journal of Engineering Mechanics, ASCE, 132(11), 1177-1186.

Cruz, P.J.S., Mari, A., and Roca, P. (1998). "Nonlinear time-dependent analysis of segmentally constructed structures", Journal of Structural Eng., ASCE, 124(3), 278-287.

Eligehausen, R., Popov, E.P., and Bertero, V.V. (1983). "Local bond stress-slip relationships of deformed bars under generalized excitations", Report No. UCB/EERC 83-23, Earthquake Engineering Research Center, University of California, Berkeley.

Filippou, F.C., Popov, E.P., and Bertero, V.V. (1983). "Effects of bond deterioration on hysteretic behavior of reinforced concrete joints", Report No. UCB/EERC-83/19, Earthquake Engineering Research Center, University of California, Berkeley.

Kang., Y.K. (1977). "Nonlinear geometric, material and time dependent analysis of reinforced and prestressed concrete frames", Report No. 77-1, SESM, University of California, Berkeley.

Kent, D.C., and Park, R. (1971). “Flexural members with confined concrete”, Journal of Structural Eng., ASCE, 97(ST7), 1969-1990.

Kodur, V.K.R., and Campbell, T.I. (1990). “Deformation controlled nonlinear analysis of prestressed concrete continuous beams”, PCI Journal, 35(5), 42-55.

Mari, A.R. (1984). “Nonlinear geometric, material and time dependent analysis of three-dimensional reinforced and prestressed concrete frames”, Report No. 84-12, SESM, University of California, Berkeley.

Menegotto, M., and Pinto, P.E. (1973). “Method of analysis for cyclically loaded reinforced concrete plane frames including changes in geometry and nonelastic behavior of elements under combined normal force and bending”, IABSE Symposium on Resistance and Ultimate Deformability of Structures Acted on by Well-Defined Repeated Loads, Final Report, Lisbon.

Mitchell, D., Cook, W.D. Khan, A.A., and Tham, T. (1993). “Influence of high strength concrete on transfer and development length of pretensioning strand”, PCI Journal, 14(4), 62-74.

Picard, A., Massicotte, B., and Bastien, J. (1995). “Relative efficiency of external prestressing”, Journal of Structural Eng., ASCE, 121 (12), 1832-1841.

Roca, P., and Mari, A.R. (1993). “Nonlinear geometric, material analysis of prestressed concrete general shell structures”, Computers and Structures, 46(5), 917-929.

Spacone, E., Filippou, F. C., and Taucer, F. F. (1996). “Fiber beam-column model for nonlinear analysis of RC frames. I: Formulation”, Earthquake Engineering and Structural Dynamics, 25(7), 711-725.

Tabatabai, H. and Dickson, T.J. (1993). “The history of the prestressing strand development length equation”, PCI Journal, 38(6), 64-75.

Yassin, Mohd H.M. (1994). “Nonlinear analysis of prestressed concrete structures under monotonic and cyclic loads”, Ph.D Dissertation, Department of Civil and Env. Eng., University of California, Berkeley.

Zienkiewicz, O. C., and Taylor, R. L. (1989). “The Finite Element Method Volume 1. Basic Formulation and Linear Problems”, Fourth Edition. McGraw Hill, London.

Notation

$\mathbf{a}(x)$ = Vector of displacement interpolation functions

$\mathbf{b}(x)$ = Vector of force interpolation functions

$\boldsymbol{D}(x)$ = Vector of forces at a distance x

$\boldsymbol{d}(x)$ = Vector of section deformations at a distance x

$\mathbf{F}$ = Element flexibility matrix

$\mathbf{f}_s(x)$ = Section flexibility matrix

h_j = Distance between centroid of concrete and tendon j

ρ_j = Perimeter for tendon j

i = Newton-Raphson iteration number

$\mathbf{K}_b$ = Bond element stiffness matrix

M = Bending moment

N_c, N_{sj} = Axial force for concrete and tendon j respectively

$\mathbf{P}$ = Vector of externally applied loads

$\mathbf{q}$ = Vector of element forces

$\boldsymbol{S}_b(x)$ = Bond-slip at distance x

$\mathbf{T}$ = coupling matrix between displacement and internal force degrees of freedom

$u_c(x),\ u_{sj}(x)$ = Concrete and tendon axial displacement respectively

$v(x)$ = transverse displacement

$\mathbf{v}$ = Vector of element displacements

$\varepsilon_c, \varepsilon_s$ = concrete and tendon axial strain respectively

χ = beam curvature

Figure Captions

Time	Operation	Model
t_0	Tendon tensioning in stressing bed	• Beam-column elements inactive • Bond elements inactive • Tendon elements active • Tensioning force applied at end node 2 of tendon • End node 1 of tendon linked to bedding element node
t_1	Transfer of prestress to concrete after it has set	• Beam-column elements active • Bond elements active • Tendon elements active • Tensioning force at end node 2 of tendon reduced to zero • Removal of bedding element from end node 1 of tendon

Table 1 Pretensioning Stages

Beam	f_c' (MPa)	f_t' (MPa)	A_p (mm^2)	P_p (mm)	f_{pi} (MPa)
16/31-1865	31.0	3.1	146.4	50.0	1286.0
16/65-1150	65.0	6.5	146.4	50.0	1218.0

Table 2 Details of Test Beam Specimens

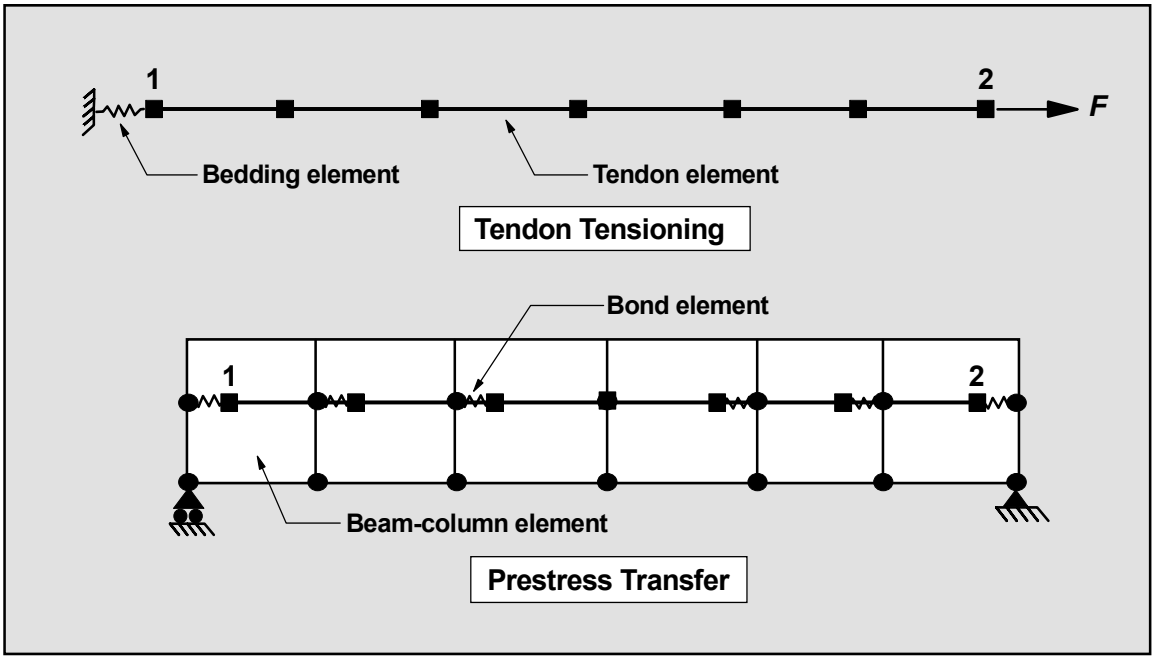

Figure 1 Pretensioning Operation

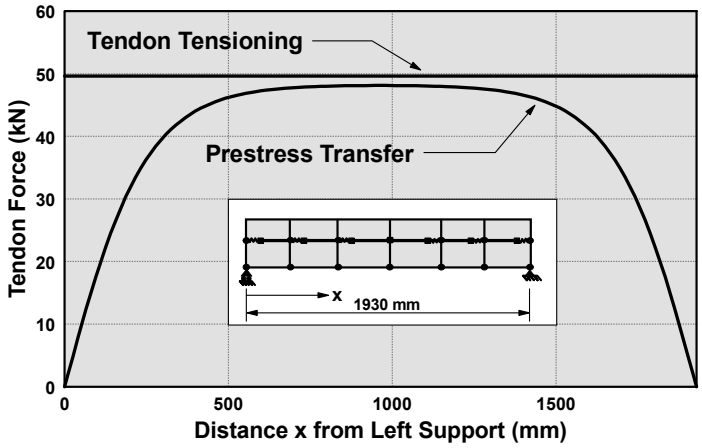

Figure 2 Analytical Tendon Force Distribution during Pretensioning

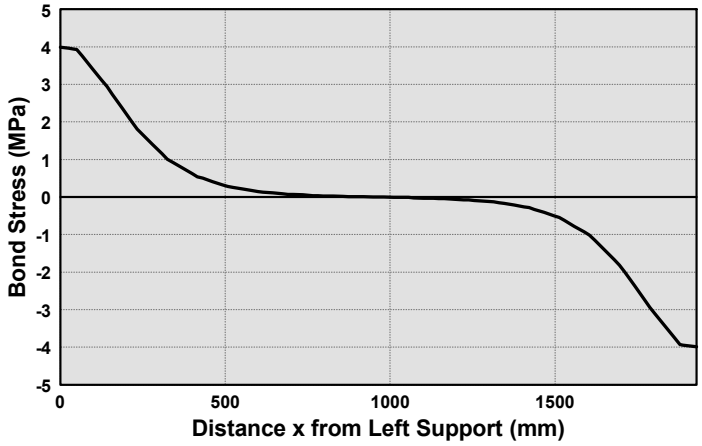

Figure 3 Analytical Bond Stress Distribution after Prestress Transfer

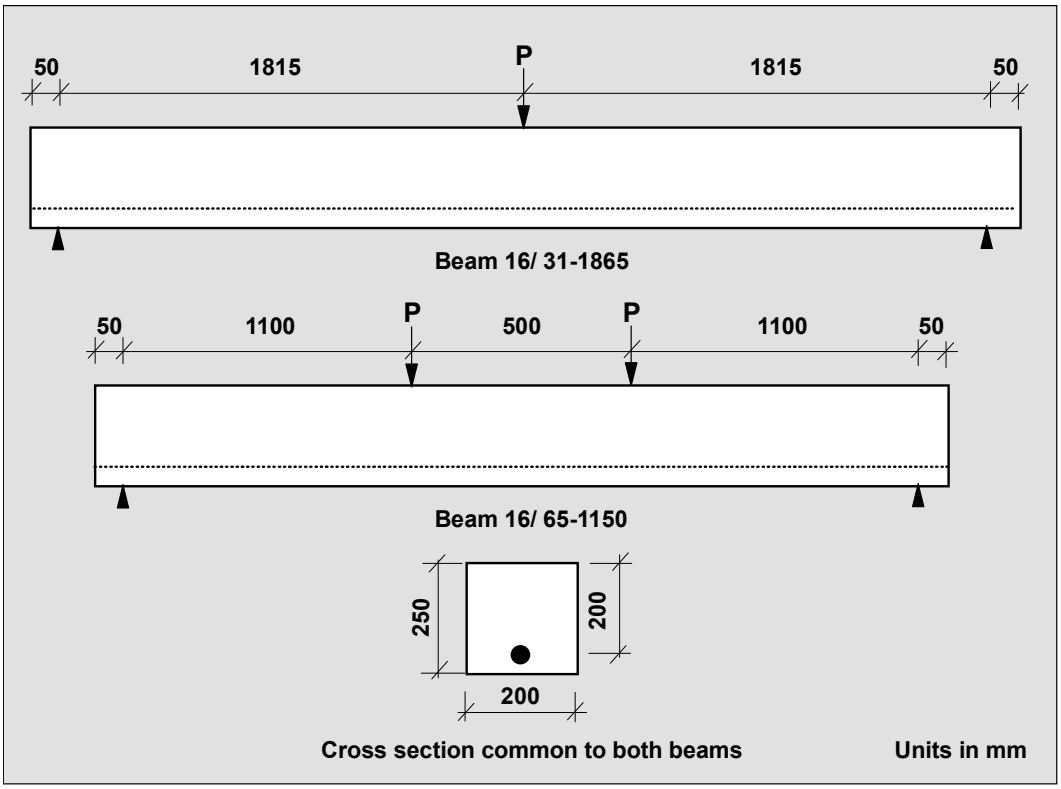

FIGURE 4 MITCHELL TEST BEAMS

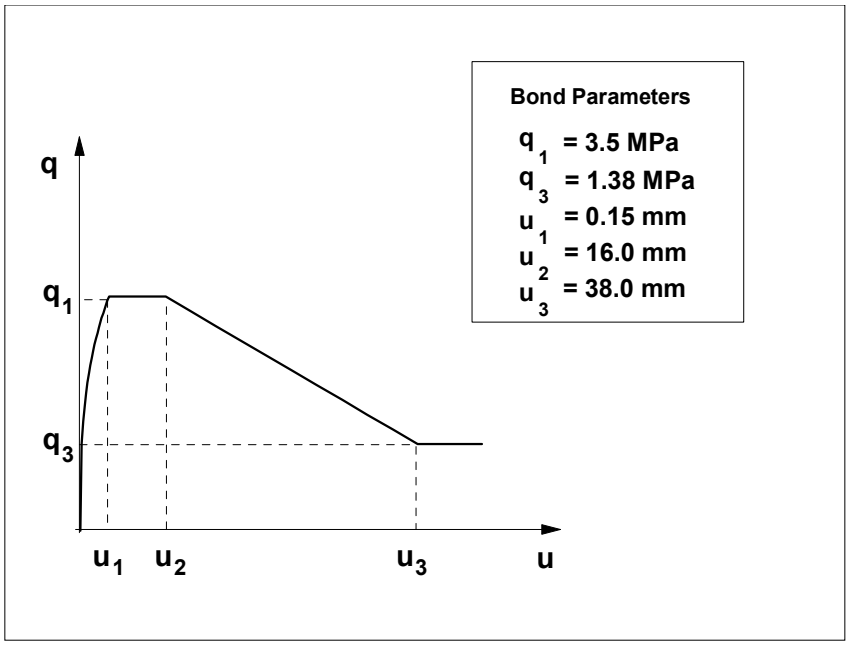

FIGURE 5 BOND PARAMETERS

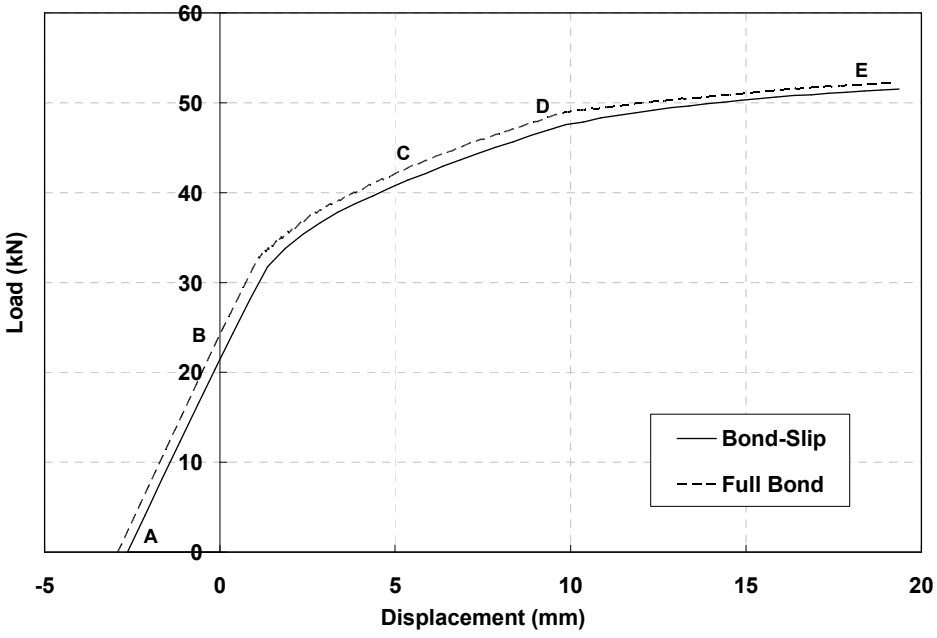

FIGURE 6 GLOBAL RESPONSE OF BEAM 16/31-1865

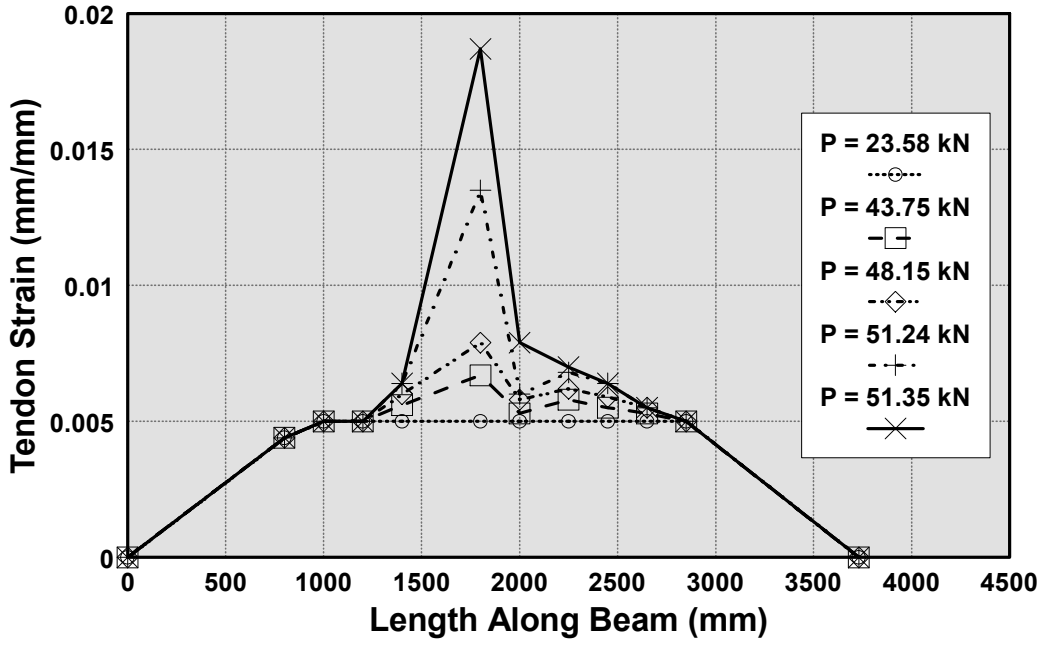

FIGURE 7 EXPERIMENTAL STRAND STRAIN DISTRIBUTION FOR BEAM 16/31-1865

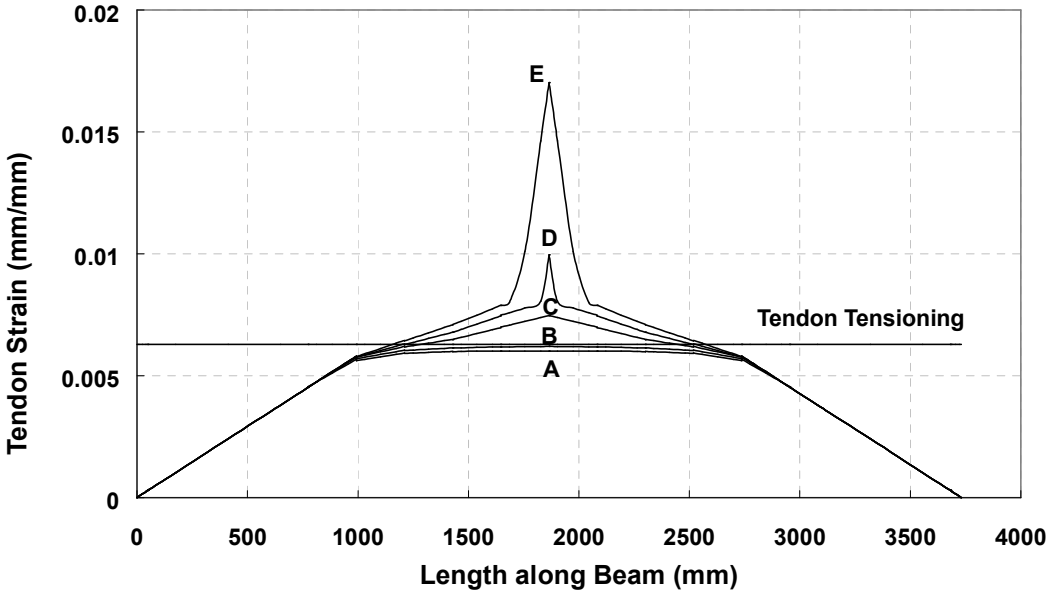

FIGURE 8 ANALYTICAL STRAND STRAIN DISTRIBUTION FOR BEAM 16/31-1865

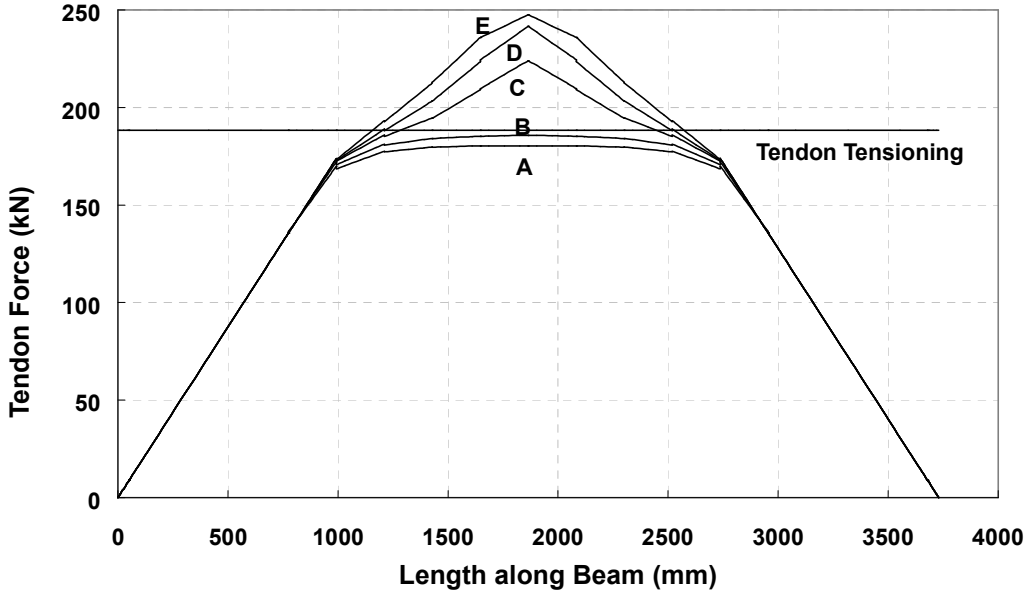

FIGURE 9 ANALYTICAL TENDON FORCE DISTRIBUTION FOR BEAM 16/31-1865 (BOND-SLIP)

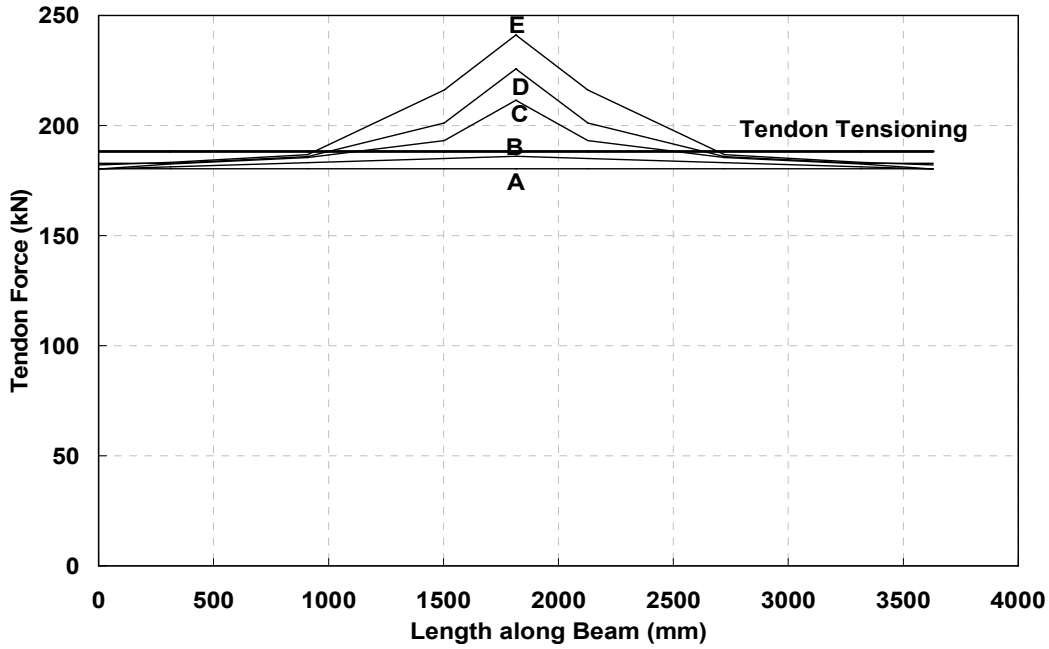

FIGURE 10 ANALYTICAL TENDON FORCE DISTRIBUTION FOR BEAM 16/31-1865 (FULL-BOND)

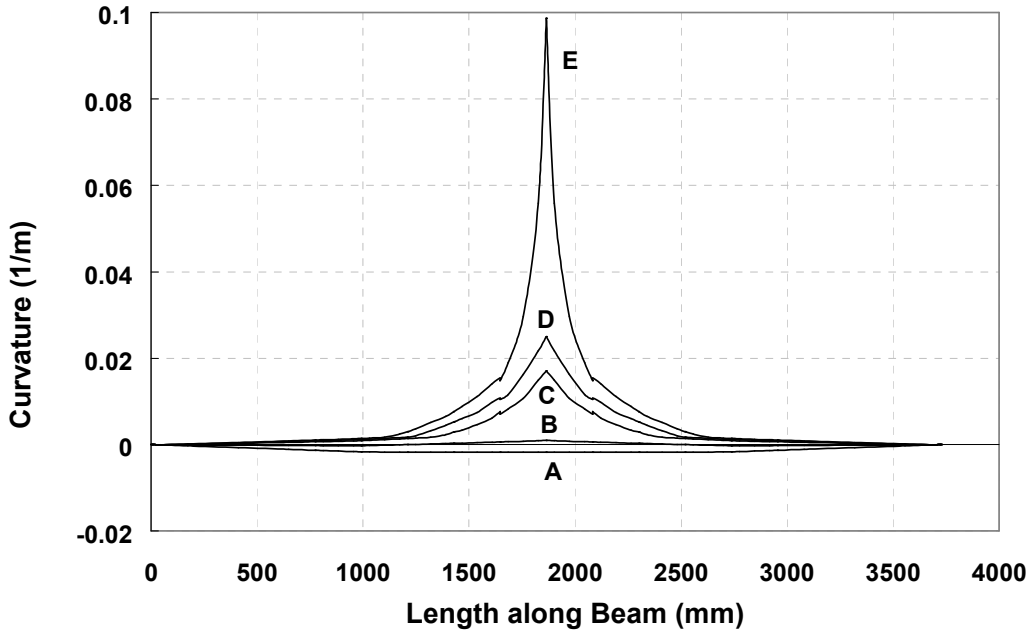

FIGURE 11 CURVATURE DISTRIBUTION FOR BEAM 16/31-1865

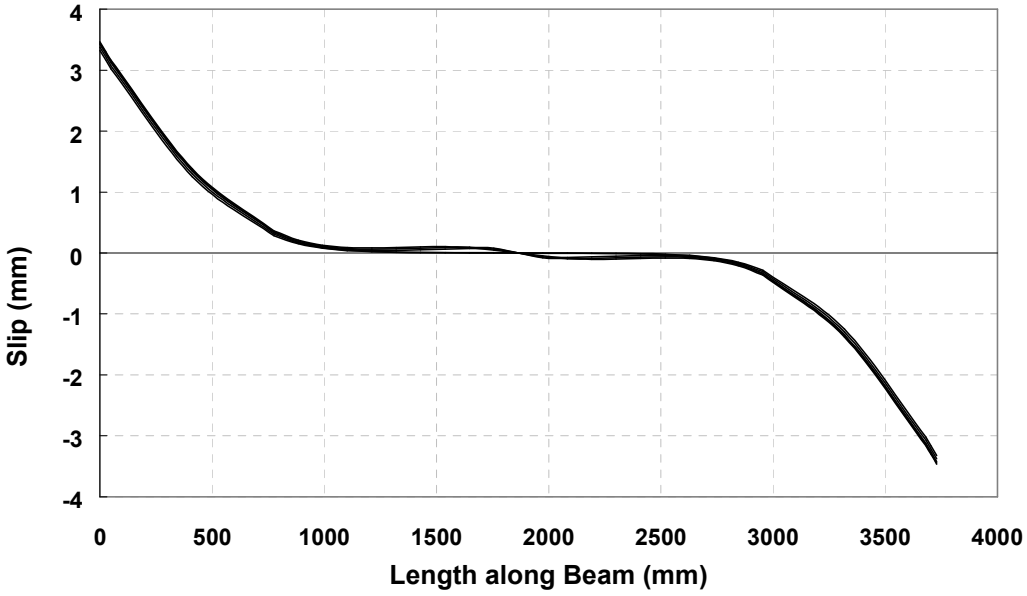

FIGURE 12 SLIP DISTRIBUTION FOR BEAM 16/31-1865

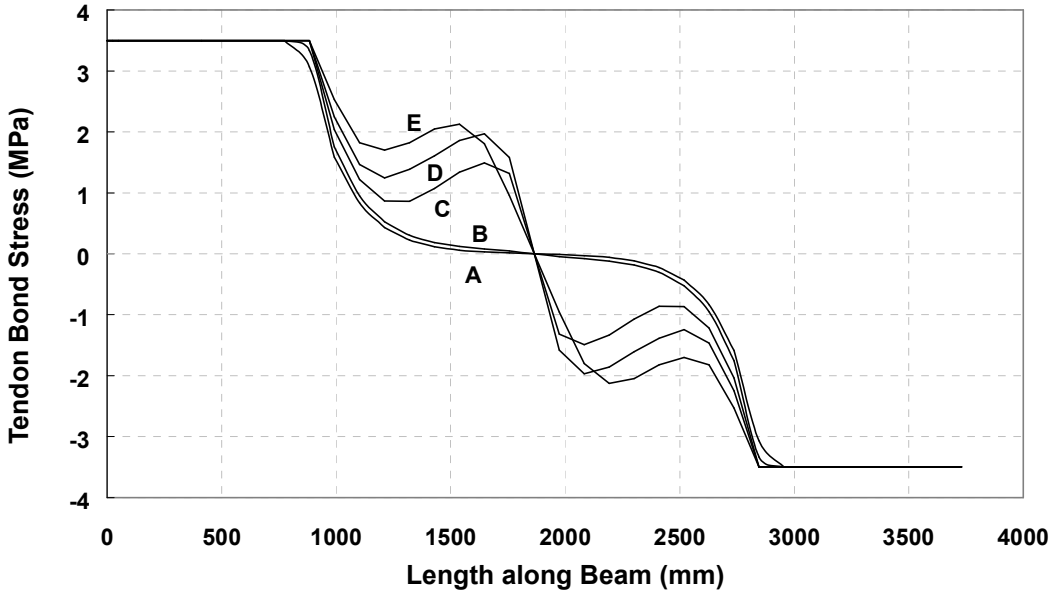

FIGURE 13 BOND DISTRIBUTION FOR BEAM 16/31-1865

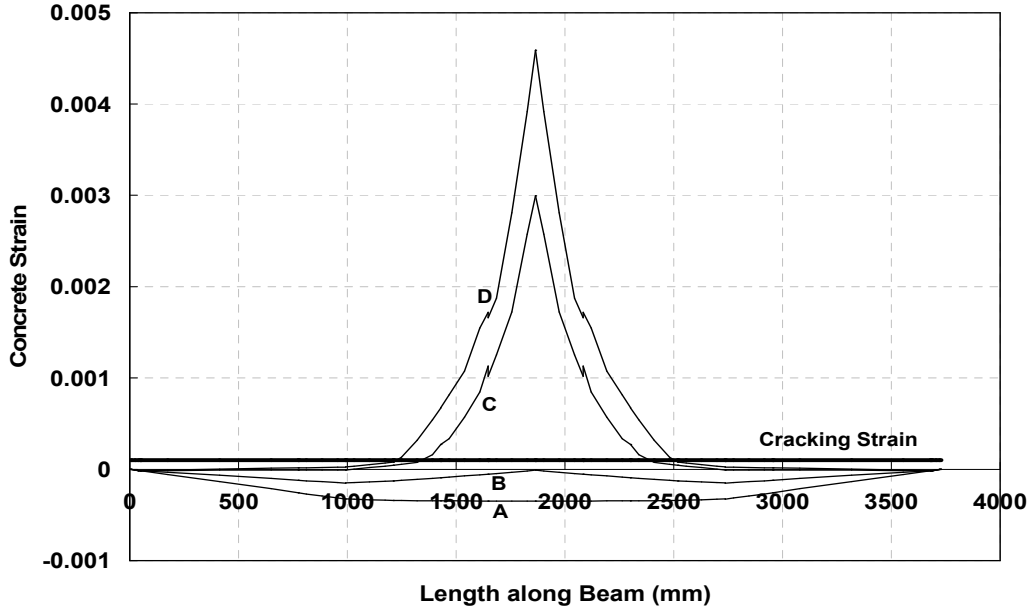

FIGURE 14 CONCRETE STRAIN DISTRIBUTION AT BOTTOM FIBER FOR BEAM 16/31-1865

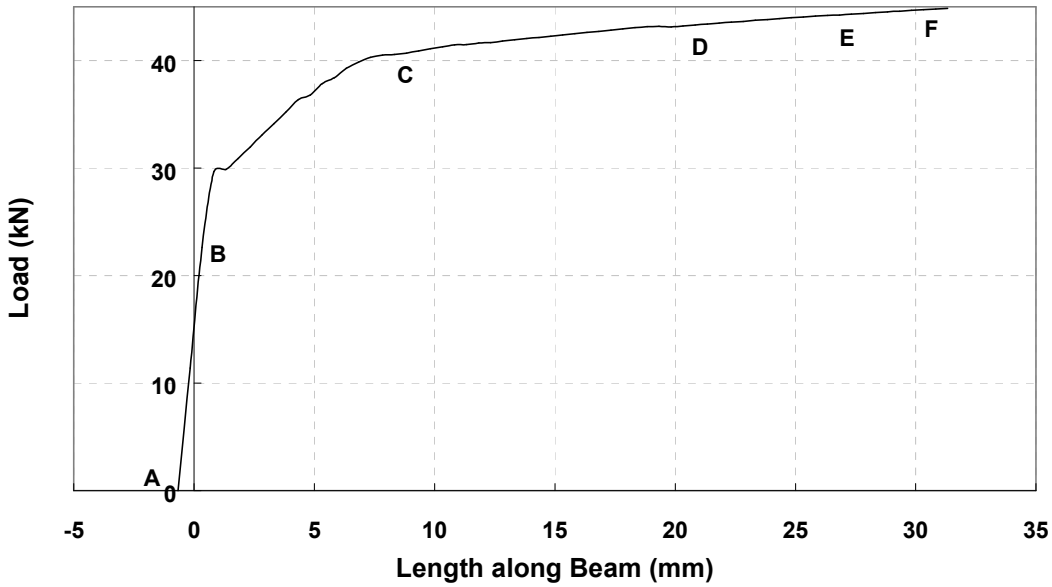

FIGURE 15 GLOBAL RESPONSE FOR BEAM 16/65-1150

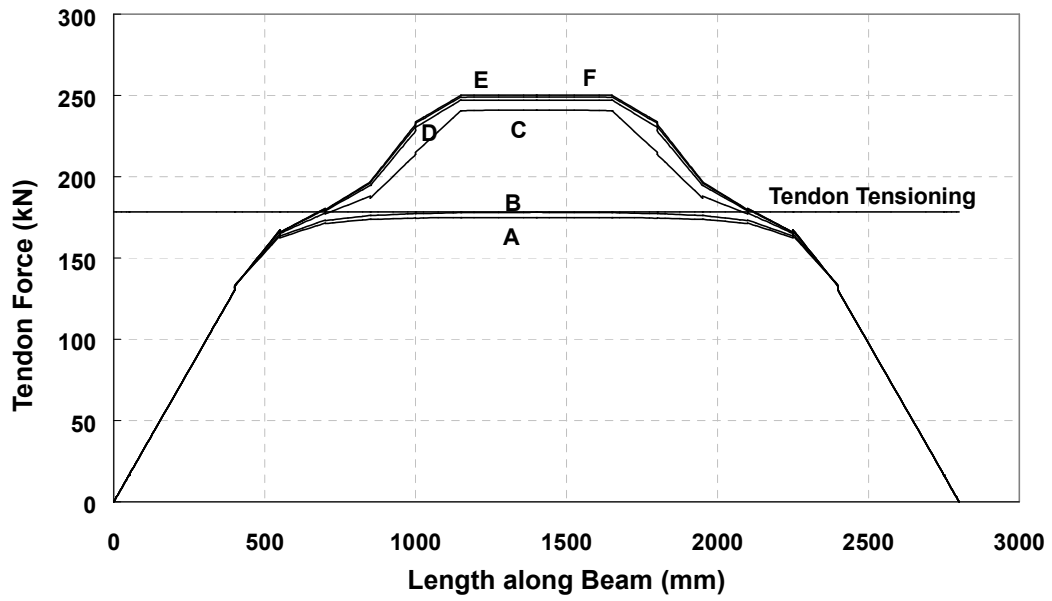

FIGURE 16 TENDON FORCE DISTRIBUTION FOR BEAM 16/65-1150

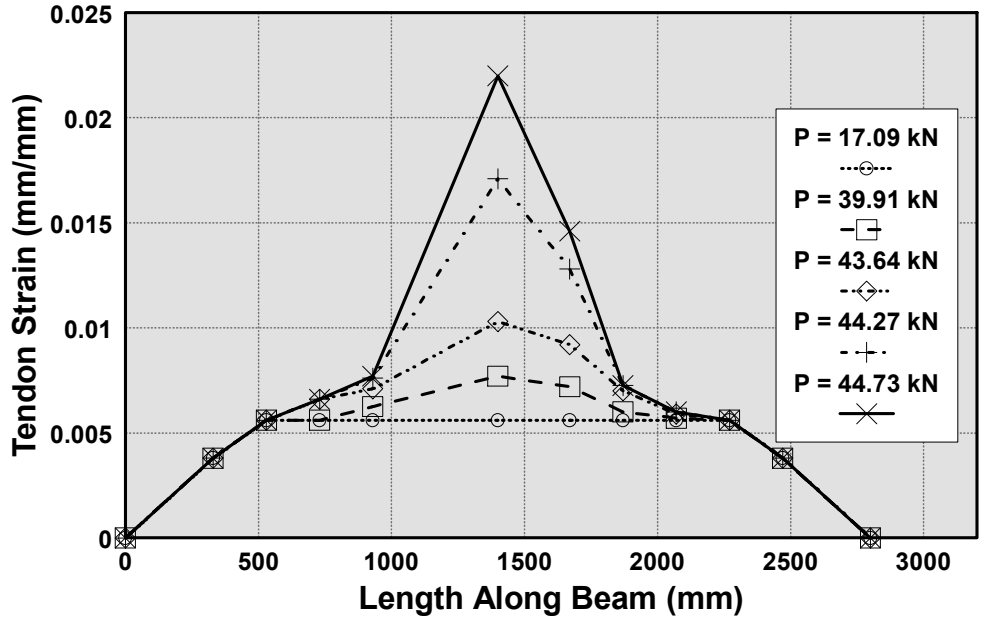

FIGURE 17 EXPERIMENTAL STRAND STRAIN DISTRIBUTION FOR BEAM 16/65-1150

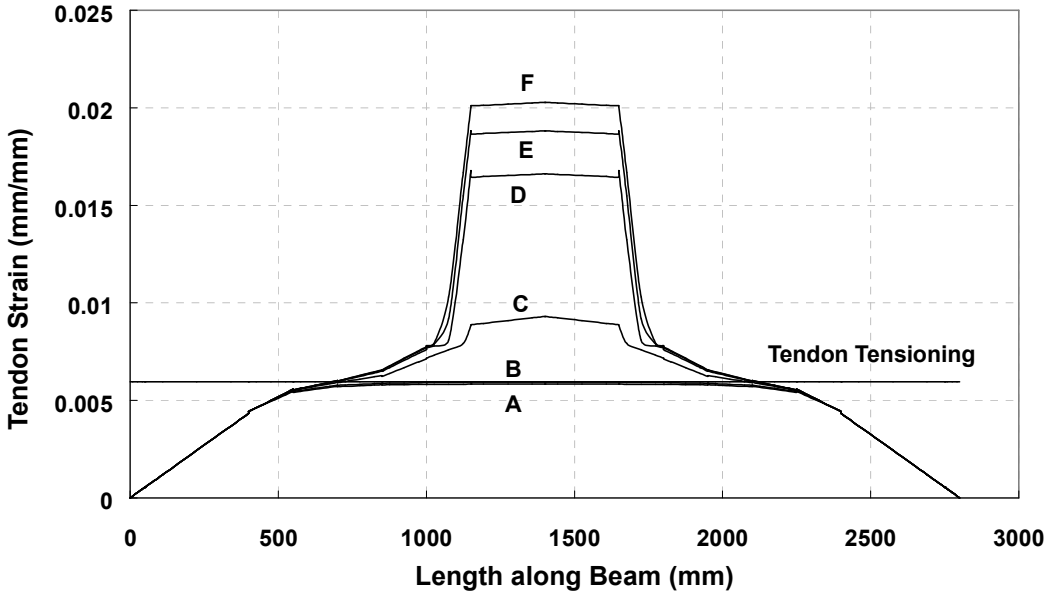

FIGURE 18 ANALYTICAL STRAND STRAIN DISTRIBUTION FOR BEAM 16/65-1150

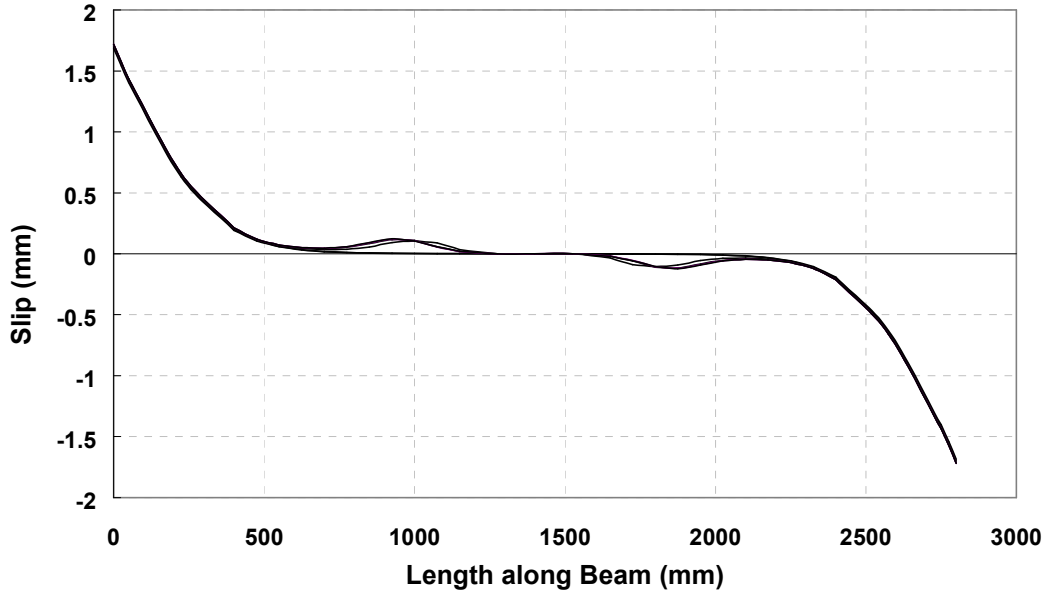

FIGURE 19 SLIP DISTRIBUTION FOR BEAM 16/65-1150

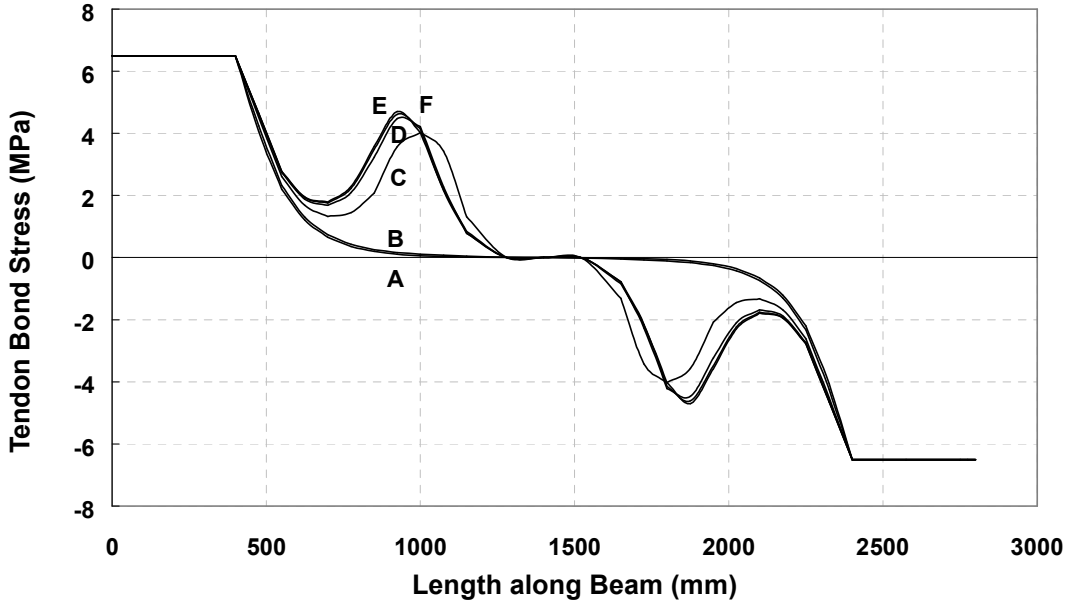

FIGURE 20 SLIP DISTRIBUTION FOR BEAM 16/65-1150

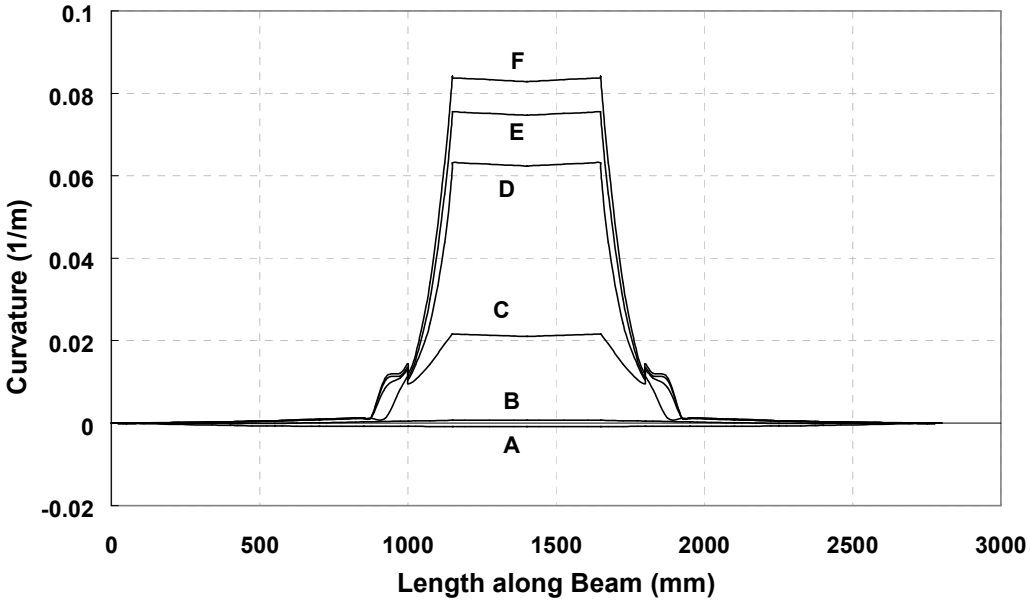

Figure 21 Curvature Distribution for Beam 16/65-1150